A Reference Atmosphere for the Atomic Sodium Layer

J. M. C. Plane[a]

[a] *School of Chemistry, University of Leeds, Leeds LS2 9JT, UK*

Abstract

The layer of Na atoms which occurs globally at a height of about 90 km is produced by the ablation of the approximately 30 tonnes of interplanetary dust which enters the atmosphere every day. The layer lies above 80 km, where there is a sufficient concentration of atomic oxygen and hydrogen to recycle sodium compounds, such as sodium bicarbonate, back to Na; and below 110 km, where the atmospheric density is high enough to convert Na^+ ions back to Na through cluster formation and dissociative electron recombination. The Na layer has been studied since the 1950s, first using ground-based photometry, then by resonance lidar, and most recently by limb-scanning spectroscopy from satellites. The data-base is now sufficient to produce a near-global reference atmosphere of the layer. Comparison is also made with the smaller data-bases of Fe, Ca and K observations.

1. Introduction

It has been known for more than seventy years that neutral metal atoms such as Na are present in the upper atmosphere. Optical emission at a wavelength of 589 nm from the transition $Na(3^2P_J - 3^2S_{1/2})$ was first reported in the Earth's nightglow spectrum in 1929 (Slipher, 1929), and within a decade it was shown that the source of this radiation was located within the Earth's upper atmosphere (Bernard, 1938). By the mid-1960s it had been established that there is a layer of sodium atoms about 10 km wide which peaks at an altitude of near 90 km (Hunten, 1967). This region is known as the mesosphere-lower thermosphere (MLT). Layers of several other metals - K, Fe and Ca - had also been observed by the mid-1970s (Plane, 1991). Figure 1 shows the annual mean profiles of these four metals, measured at mid-latitude observatories in the northern hemisphere. These observations raise several obvious questions: what is the source of the metals, extra-terrestrial or from the Earth's surface; why do the metals occur as layers of highly reactive neutral metal atoms, and why are these layers only a few kilometres thick? More generally: are the metal layers useful tracers of dynamical processes such as gravity waves and tides; do the metals have any impact in the stratosphere and troposphere; and how are the layers affected by longer-term trends such as the solar cycle and anthropogenic climate change?

Answers to these questions require a detailed understanding of the chemistry which these metals undergo in the upper atmosphere (Plane, 2003), so that atmospheric models can be developed and tested against observation. Substantial progress has been made during the last 25 years, through laboratory studies of the reactions which metal atoms, ions and molecules undergo with atmospheric species such as O_3, O_2, O, H etc. (Plane, 2002). This has led to atmospheric models of the Na, Fe, K and Ca layers which successfully reproduce many characteristic features (Plane, 1991; Eska et al., 1999; Gerding et al., 2000; McNeil et al., 2002; Plane, 2003, 2004; Gardner et al., 2005).

The purpose of this paper is to present a reference atmosphere of the global Na layer. This is the only metal for which there is a near-global set of observations, and is also the metal whose atmospheric chemistry has been most studied and is best understood (Plane, 2004). In order to provide some background to the development of the Na climatology, it is necessary first to review the current knowledge about the source of the mesospheric metals, the chemistry which causes the layers of metal atoms to occur in the MLT, and the ground-based and space-borne techniques which have been used to observe the Na layer.

2. Meteoric ablation as the source of mesospheric metals

The two principal sources of meteoroids in the Earth's atmosphere are the dust trails produced by sublimating comets as they orbit the sun, and fragments from the asteroid belt beyond Mars (Ceplecha et al., 1998; Williams, 2002). Because of their very high entry velocities (11 - 72 km s^{-1}), meteoroids undergo rapid frictional heating by collision with air molecules, leading to vaporization of their constituent minerals. This process provides the major source of the metals (and silicon) in the MLT (Plane, 2003). The input flux of meteoroids into the atmosphere is rather uncertain, because no single technique can observe particles over the mass range from about 10^{-10} to 10^{-3} g which make up the bulk of the incoming material (Ceplecha et al., 1998). Until the 1990s, a commonly assumed figure for the daily mass input was 44 t d^{-1}, integrated over the entire Earth (Hughes, 1997). This estimate was made by extrapolating from the input flux for visual meteors (mass > 10 mg) to the flux derived from satellite impact data (mass < 1 μg), and ignoring indications of a somewhat lower flux from measurements made by conventional meteor radars, which measure specular reflections from the ion trail created in the atmosphere by the ablating meteoroid. A somewhat larger estimate of 110 ± 55 t d^{-1} was then derived from analysis of small particle impact craters on the Long Duration Exposure Facility (LDEF), an orbital impact detector placed on a spacecraft for several years (Love and Brownlee, 1993). However, in the LDEF experiment the measured crater size was treated as a proxy for particle kinetic energy, and so the mass distribution was derived by assuming the particle velocity distribution peaked around 18 km s^{-1}. More recently, high-power large aperture radars have reported direct observations of the meteor head echo (i.e. the ball of plasma around the ablating particle as it descends through the atmosphere). This enables measurements of the direction of the line-of-sight velocity, deceleration and meteoroid mass to be made, and resulted in an estimate of the total incoming mass that is about 1 order of magnitude lower than the LDEF estimate (Janches et al., 2000). However, the magnitude of the head echo is highly dependent on the meteoroid mass and velocity, so that this technique is biased to faster particles (Dyrud et al., 2005).

The mass flux has also been estimated using the accumulation of cosmic elements in the atmosphere or at the surface. Single-particle analyses of stratospheric aerosol have shown that half of the particles in the lower stratosphere contain 0.5 to 1.0% meteoric iron by mass, requiring a total extraterrestrial flux of between 20 and 100 t d^{-1} (Cziczo et al., 2001). Measurements of the accumulation of Ir and Pt in polar ice cores have been used to deduce a mass flux of 40 ± 16 t d^{-1} (Gabrielli et al., 2004), and measurements of supermagnetism from cosmic Fe in ice cores indicate a flux of 35 ± 10 t d^{-1} (Lanci et al., 2007). Finally, a recent model of the mesospheric Na layer requires a flux of 10 – 30 t d^{-1} to match lidar observations of the layer (Plane, 2004).

A consensus around 20 – 40 t d^{-1} has therefore emerged in the last 5 years. However, this estimate is a global average which does not take account of seasonal and latitudinal variations. A new meteoroid input flux (MIF) model has been developed recently (Janches et al., 2006), which assumes that the incoming particles originate from an Earth's Apex-centered particle population (~70%), and secondary Helion and Antihelion populations (~30%). The MIF model compares well with radar observations of meteors over a range of latitudes and season (Janches et al., 2006). The model predicts that the meteor flux is a minimum in spring (i.e. March/April in the northern hemisphere, September/October in the southern hemisphere), and a maximum in autumn. The seasonal ratio increases from ~1.2 in the tropics to ~15 in the polar regions (Janches et al., 2006).

Current meteoric ablation models assume that most of the extra-terrestrial material has the composition of ordinary chondrites (Vondrak et al., 2008), so that the major metallic constituents by elemental atomic abundance are then: Mg 14.4%, Si 13.6%, Fe 12.1%, Al 1.2%, Ca 0.82% and Na 0.80% (Mason, 1971; Sears and Dodd, 1988). Differential ablation is also assumed to occur. That is, the relatively volatile elements such as Na and K evaporate first, followed by the bulk constituents Fe, Mg and Si, and finally the refractory elements such as Ca (McNeil et al., 1998; Vondrak et al., 2008). Figure 2 illustrates the total injection rate of individual elements, integrated over the LDEF meteoroid mass and velocity distributions (Vondrak et al., 2008). This shows that the alkali metals Na and K are released around 93 km (i.e., the centroid heights of their ablation profiles), approximately 10 km above the major meteoric components. About 92% of the incoming Na evaporates as Na atoms, and approximately 50% of these are immediately ionized by hyperthermal collisions with air molecules (Vondrak et al., 2008).

3. The chemistry of sodium in the MLT

Meteoric ablation thus injects Na atoms and Na^+ ions directly into the region where the Na layer occurs. These species then undergo the neutral and ion-molecule chemistry illustrated in Figure 3. Na atoms are rapidly oxidised by a series of reactions involving O_3, O_2, H_2O and CO_2 to the dominant reservoir species, sodium bicarbonate ($NaHCO_3$). However, this species, as well as other Na-containing molecules such as NaO, NaO, NaO_2 and NaOH, react with either atomic O or H (and, to a lesser extent, undergo daytime photolysis) to regenerate Na. Thus, the atomic Na layer only appears above 80 km, where atomic O and H increase by several orders of magnitude and are present both during the day *and* at night (Plane, 2003). This ensures rapid recycling of sodium between Na and $NaHCO_3$. The small scale height of 2 - 3 km (the scale height is the distance over which the concentration changes by a factor of *e*) on the underside of the Na layer (Figure 1) closely follows the atomic O fall-off. Below about 85 km the $NaHCO_3$ is also permanently lost by condensation onto meteoric smoke particles. These are approximately 1 nm-size particles which form from the polymerization of metal oxides, carbonates and silicates produced by meteoric ablation (Hunten et al., 1980; Kalashnikova et al., 2000; Megner et al., 2006; Saunders and Plane, 2006; Bardeen et al., 2008). Meteoric smoke particles also probably provide ice nuclei for the formation of noctilucent clouds in the summer high-latitude mesosphere (Megner et al., 2006; Bardeen et al., 2008). The ice particles in these clouds, with radii of ~50 nm, remove sodium species even more efficiently (Gardner et al., 2005; Murray and Plane, 2005).

Above 95 km, in the lower *E* region of the ionosphere, there is a marked increase in the concentration of plasma, which consists mostly of NO^+, O_2^+, and electrons (Plane, 2003). As shown in Figure 2, Na atoms charge exchange readily with these positive ions to form Na^+, because of the low ionization potential of Na (5.3 eV). Photo-ionization is a less important ionization pathway. Na^+ then forms a cluster with N_2. Although the $Na^+.N_2$ cluster ion is not strongly bound and tends to recycle to Na^+ via reaction with atomic O, eventually it switches with CO_2 or H_2O to form strongly-bound cluster ions which undergo dissociative recombination with electrons to yield neutral Na. The $Na^+.N_2$ cluster ion forms through a pressure-dependent association reaction. Hence, the top-side of the Na layer (also only 2 - 3 km, see Figure 1) is controlled by the decrease in atmospheric pressure and the increase of plasma density. To summarise, the Na layer appears as a thin layer at about 90 km because there are significant concentrations of atomic O and H throughout day and night above 85 km to prevent the formation of molecular Na-containing species, and the plasma density is relatively low and the atmospheric pressure is high enough below 100 km to prevent a build-up of Na^+ ions.

4. Observational techniques

The first quantitative observations of metal atoms in the MLT were made in the 1950s using ground-based photometers. These instruments measured the resonance fluorescence from spectroscopic transitions of Na, K, Fe and Ca^+ atoms excited by solar radiation (Hunten, 1967). The emission lines can be observed successfully because these metals have extremely large resonant scattering cross-sections, which is necessary because their concentrations relative to the general atmosphere are less than 100 parts per trillion. Vertical profiles of the metals were obtained by measuring the fluorescence signal as a function of solar zenith angle, while the solar terminator passed through the MLT at twilight.

Photometry was superseded in the 1970s following the invention of the laser and the development of the resonance lidar technique (Bowman et al., 1969; Plane, 1991). A pulsed laser beam, tuned to a strongly allowed spectroscopic transition of the metal atom of interest, is transmitted up through the atmosphere. In the MLT the pulse is then resonantly scattered by the metal atoms. A small fraction of the scattered light returns to the ground, where it is collected by a telescope and measured by time-resolved photon counting. The return signal is electronically binned to provide the range, and hence the height, of the scattering layer. The absolute metal density is calibrated from the Rayleigh-scattered signal at a lower altitude of known atmospheric temperature and density. Lidar has so far been used to observe Na, K, Li, Ca, Ca^+ and Fe (Plane, 1991, 2003). Observations can even be made continuously over a complete diurnal cycle, provided an astronomical quality telescope and narrow band optical filter are employed for daytime measurements. Observations can also be made with extremely good temporal and height resolution (typically 60 s and 40 m, respectively, for the Na layer), so that the metal layers can be used as tracers of atmospheric motions such as tides and gravity waves. In the case of Na and K, a narrow line-width laser can be used in the lidar transmitter to measure temperature and wind profiles in the upper mesosphere (States and Gardner, 2000; Yuan et al., 2006; Höffner and Lübken, 2007). Resonance metal lidars have thus become extremely important tools for studying the chemistry and physics of the MLT. Figure

4 illustrates the worldwide locations of lidar observatories where significant data-sets on the metal layers have been obtained.

There have also been measurements of the concentrations of positive metallic ions made by rocket-borne mass spectrometry (Kopp, 1997; Grebowsky and Bilitza, 1999; Grebowsky and Aikin, 2002). Metallic ions such as Mg^+ and Fe^+ have also been observed by resonant scattering of sunlight using spectrometers on space vehicles (Gardner et al., 1999; Grebowsky and Aikin, 2002; Scharringhausen et al., 2008). The first satellite-borne observations of the sodium nightglow were made two decades ago (Newman, 1988). However, the emission was several km lower than expected, probably because of a satellite altitude-pointing error (Clemesha et al., 1990). In any case, a fundamental difficulty with using the nightglow to measure the atomic Na density is that the emission is actually produced by chemiluminescence from a fast cycle initiated by the reaction between Na and O_3, and is thus not a direct measure of the Na atom concentration (Plane, 2003). More recently, global measurement of the mesospheric sodium layer were obtained by stellar occultation measurements using the GOMOS instrument on the ENVISAT satellite (Fussen et al., 2004). An important advantage of occultation is that the absolute Na density is derived straightforwardly from the absorption cross section, although the Na layer is optically thick over a path length of several hundred km and this may have led to poor agreement of the retrieved Na column abundance, layer density profile and the seasonal and latitudinal variation, compared with ground-based lidar measurements (Fan et al., 2007b).

Most recently, a new mesospheric Na retrieval method has been developed to derive Na density profiles from satellite limb-scanning measurements of the Na resonance emission line in the dayglow (Gumbel et al., 2007). Observations were made from the Odin satellite using the OSIRIS spectrograph, which measures irradiance in the limb at wavelengths between 280 and 800 nm with a resolution of ~1 nm. The Na dayglow radiance profile was then inverted into the absolute Na density profile using optimal estimation theory, and validated against simultaneous ground-based Na lidar measurements (Fan et al., 2007b).

5. Development of a Na Reference Atmosphere

The reference atmosphere presented in this section consists of zonally-averaged data in 10^o latitude bins, on a monthly timescale. The reference atmosphere has been constructed from several data-sets. The recent OSIRIS/Odin data-set (Fan et al., 2007b) provides a near-global set of measurements. Because the data is self-consistent and ground-truthed to lidar observations (Gumbel et al., 2007), it forms the backbone of the reference atmosphere. However, there are some limitations. First, the data covers only two complete years, 2003 and 2004. Second, the sun-synchronous orbit of Odin provided measurements only at ~0600 and 1800 hrs local time. Since the Na layer is subject to photochemical and tidally-driven diurnal variations (Clemesha et al., 1982; Fan et al., 2007b), the data from both local times has been averaged. Third, the dayglow spectroscopic measurements are restricted to periods when the mesosphere is illuminated (solar zenith angle < 92^o), and so there is no data at mid- to high latitudes during winter. In order to partly overcome these limitations, lidar data from the South Pole for the years 1995-1997 (Gardner et al., 2005), from São José dos Campos (23°S) for the years 1972-1986 (Clemesha et al., 1992b1992a; Clemesha et al., 2004), and Urbana-Champaign (40^oN) and Ft. Collins (41^oN) for the years 1991-1999 (Plane et al., 1999; States and Gardner, 1999; She, 2000) has been

included. Lidar data from other observatories (Figure 4) is either already covered by the satellite measurements, or has not yet been published as a long-term record. It should be noted that the uncertainty in the absolute Na density near the layer peak retrieved from OSIRIS/Odin is about ± 10% (Gumbel et al., 2007), similar to modern ground-based lidars. However, the natural variability of the Na layer means that the average monthly column abundance and peak density values in some of the 10^o latitude bins have a larger uncertainty (up to ±30%), depending on the number of profiles in the average (Fan et al., 2007b).

Although these data-sets are taken from different decades and phases of the solar cycle, a long-term study of the Na layer (Clemesha et al., 1992b; Clemesha et al., 2004) shows that, at least at low latitudes (23^oS), the effects of changing climate and the solar cycle on the Na layer are small. The centroid of the layer moves down only 0.17 ± 0.11 km between solar min and max. This downward trend is probably due to changes in the diurnal tide (Clemesha et al., 1992b) and chemistry: at solar max there is a greater plasma density in the lower *E* region, so more Na is converted to Na^+ on the topside (Figure 3), whereas higher atomic H (and O) concentrations below 90 km (produced by increased Lyman-α radiation) recycle Na from $NaHCO_3$ more rapidly on the underside of the layer. Measurements made at Urbana-Champaign, Illinois (40^oN) between 1991-94 (Plane et al., 1999) and 1996-98 (States and Gardner, 1999), which correspond to periods at and shortly after solar max and min, respectively, show that the Na column abundance was about 20% higher at solar max.

Table 1 lists the Na column abundance, as a function of latitude and month, which is shown as the contour plot in Figure 5. The average column abundance is 3.9 x 10^9 atom cm^{-2}, although this ranges by a factor of 20 (0.33 - 7.4 x 10^9 atom cm^{-2}), depending on time and location. The layer exhibits a seasonal variation with an early wintertime maximum: October-November in the northern hemisphere (Plane et al., 1999), and April in the southern hemisphere (Clemesha et al., 1979). The size of the variation is latitude-dependent: at low latitudes the winter enhancement is only a factor of about 1.3 (Simonich et al., 1979) (Clemesha et al., 1979), whereas at mid-latitudes the wintertime enhancement is approximately a factor of 3 (Plane et al., 1999), and more than 10 in the polar regions (Gardner et al., 1988; Kurzawa and von Zahn, 1990; Gardner et al., 2005).

The top panel of Figure 6 illustrates this substantial increase in the seasonal variability from equator to pole. The increase is caused by several factors. First, the sodium chemistry is sensitive to temperature (Plane et al., 1998b): in particular, the reaction between $NaHCO_3$ and H has a significant activation energy, and so $NaHCO_3$ is a more stable reservoir at lower temperatures (Cox et al., 2001). This causes the Na abundance to decrease with temperature, and the summertime temperature minimum to get colder towards the poles (Plane, 2003). Second, the summertime temperature falls below 150 K at latitudes higher than ~55^o, resulting in the formation of noctilucent clouds. The ice surface in these clouds is large enough to remove the metallic species more rapidly than they are replenished by meteoric ablation or vertical transport, leading to near complete removal of Na below 90 km (Gardner et al., 2005). Third, there is a pronounced meridional circulation in the mesosphere from summer pole to winter pole. The resulting convergence of lower-latitude air over the winter polar vortex leads to an enhancement of Na (Gardner et al., 2005). The Antarctic vortex has a stronger and more consistent circulation than the Arctic vortex, with the result that the wintertime Na layer over Antarctica has the highest column abundance globally (Figure 5). Conversely, noctilucent clouds form more frequently

in the Arctic (DeLand et al., 2007), and so this is where the global minimum Na abundance is observed (Table 1). Inspection of Figure 5 shows that the summertime minimum in Na abundance occurs about 2 weeks after solstice, which coincides with the maximum occurrence frequency of the clouds (DeLand et al., 2007). Fourth, the meteoric influx peaks in autumn and minimises in spring, with a seasonal variation that is about an order of magnitude larger at high latitudes compared with the tropics (Janches et al., 2006). This probably contributes to the early winter maximum in Na abundance seen at latitudes higher than about 40^{o}N.

The peak density, peak height and FWHM (full width at half maximum) of the Na layer are listed as a function of latitude and season in Tables 2 - 4. Like the column abundance, the peak density is smallest in the northern hemisphere summer at 80^{o}N (770 cm^{-3}), when the layer is relatively narrow (FWHM = 4.8 km) and high (peak height = 92.0 km) because of the removal of sodium species by noctilucent clouds below 87 km. The summertime layer at South Pole in December is even higher (93.7 km) and narrower (3.9 km). In contrast, the highest Na peak density (5740 cm^{-3}) occurs in the winter at South Pole, as a result of warm temperatures and convergence of the meridional circulation. The layer is also much broader (FWHM = 10 - 13 km) and lower (88 - 89 km). Figure 6 (bottom panel) and Figure 7 compare the seasonal variations in the peak density, peak height and FWHM at the equator and South Pole. As in the case of the column abundance, the seasonal changes in all these parameters become much greater at high latitude.

Finally, although the reference atmosphere presented here describes the global "background" Na layer, it is important to mention the phenomenon of sporadic (or sudden) neutral Na layers (SSLs). These are thin layers (FWHM ~1 km) of relatively high concentrations of Na atoms that appear and disappear abruptly. They occur at altitudes between 95 - 105 km, on the topside of the normal Na layer (Clemesha, 1995). Their peak concentration can be more than 40 times the peak of the background metal layer (Kane et al., 1993). Airborne lidar observations have also shown that SSLs can have a horizontal extent of more than 1000 km (Kane et al., 1991). Indeed, satellite observations indicate that these layers can very occasionally extend over more than 50^{o} in latitude (Fan et al., 2007a). The explanation for most SSLs appears to be neutralization of Na^{+} ions in a descending sporadic *E* layer (Hansen and von Zahn, 1990; Kane et al., 1993; Cox and Plane, 1998). The high correlation between SSLs and sporadic *E* layers (Batista et al., 1989; Hansen and von Zahn, 1990; Mathews et al., 1993; Nagasawa and Abo, 1995; Heinselman et al., 1998; Collins et al., 2002; Gong et al., 2002; Williams et al., 2007) provides compelling evidence that the neutralization of Na^{+} is an important mechanism of SSL formation, particularly as this theory is now supported by laboratory studies of the relevant ion-molecule reaction kinetics (Cox and Plane, 1997) and atmospheric modelling (Cox and Plane, 1998; Heinselman, 2000; Collins et al., 2002).

SSLs layers were first reported in 1978 at 23^{o}S (Clemesha et al., 1978). Subsequent measurements at other latitudes have shown that the SSL occurrence frequency is highly variable. In the northern hemisphere , SSLs are frequently observed in polar regions (Hansen and von Zahn, 1990; Heinselman et al., 1998; Plane et al., 1998a; Williams et al., 2007) and latitudes below 20^{o}N (Kwon et al., 1988; Beatty et al., 1989; Kane et al., 1991; Kane et al., 1993; Mathews et al., 1993). At northern hemisphere middle latitudes, however, the situation is more complex. Regular observations of the mesospheric Na layer have been made in the mid-latitude US at 40^{o}N (Gardner et al., 1986) and Europe at 44^{o}N (Gibson and Sandford, 1971; Megie and Blamont, 1977) since the 1970s, but SSLs have rarely been observed. In

contrast, there is a relatively high SSL occurrence over Japan at 36°N (Nagasawa and Abo, 1995) and southern China at 31°N (Gong et al., 2002). SSLs have also been observed in the southern hemisphere equatorial region (2°S) (Clemesha et al., 1998), and at low latitudes (23°S) (Batista et al., 1989). Most recently, space-borne observations of SSLs from OSIRIS/Odin show that the greatest occurrence frequency of these layers is around the southern tip of South America and the Antarctic peninsula, possibly related to the extreme gravity wave momentum flux in this region (Fan et al., 2007a).

6. Comparison of Na with the Fe, Ca and K layers

Figure 8 illustrates the Na, Fe, K and Ca layers as a function of height and month, observed by lidar at several mid-latitude locations (40 - 54°N) where observations have been made over at least one annual cycle (Gerding et al., 2000). Like Na, the mid-latitude Fe layer exhibits an early winter maximum and mid-summer minimum in concentration (Kane and Gardner, 1993; Helmer et al., 1998). Similar behaviour, though with a larger seasonal variation (factor of ~3), has been observed in the Fe layer at South Pole (Gardner et al., 2005). At 30°N (Yi et al., 2009) and 18°N (Raizada and Tepley 2003), the seasonal variation is smaller than at mid-latitudes, analogous to the low-latitude Na layer in Figure 5. In contrast to Na and Fe, Figure 8 shows that the mid-latitude K and Ca layers have a semi-annual variation with a pronounced second maximum in mid-summer (Eska et al., 1998; Eska et al., 1999; Gerding et al., 2000). This is especially surprising in the case of K, which might be expected to behave most like Na. Differences in the ion-molecule chemistry of these alkali metals may be the explanation (Plane et al., 2006). A meridional profile of the K layer has been obtained between 71°S and 45°N using a shipboard K lidar (Eska et al., 1999). This showed a ten-fold increase in both the K peak density and column abundance when going from the Antarctic to the equator.

There are other interesting differences in the layers. Compared with the peak of the Na layer, the K peak is on average 1.2 km lower (Eska et al., 1998). The Ca peak height at mid-latitudes moves from about 92 km in winter to 88 km in summer (Gerding et al., 2000), which is the reverse of the Na layer. At mid-latitudes, the Fe peak is about 4 km below that of Na, and the Fe layer also has an extremely small bottom scale-height (< 1 km) compared with the Na layer (Figure 1). The peak height of Fe is about 87 km in summer and winter, and about 2 km higher in spring and autumn (Kane and Gardner, 1993). At high latitudes, the Fe peak height is more variable, extending from 83 km in winter to 91 km in summer (Alpers et al., 1993; Gardner et al., 2005).

The most dramatic result in Figure 8 (see also Figure 1) is the enormous depletion of Ca relative to Na by a factor of 120 - 360 depending on season (Gerding et al., 2000), since these elements have almost identical elemental abundances in chondritic meteoroids (see Section 2). There is also a more modest depletion of Fe by a factor of about 8 (Helmer et al., 1998; Plane, 2003). In both cases these depletions, relative to their cosmic abundances, do not seem to be explained by differential ablation: a recent differential ablation model (Figure 2) indicates that Ca and Fe should be depleted relative to Na by factors of only 4 and 1.2, respectively (Vondrak et al., 2008). In the case of calcium, both Ca and Ca^+ can be monitored simultaneously by lidar, and this has permitted the relationship between the metal atoms and ions to be studied in some detail (Gerding et al., 2000; Gerding et al.,

2001). The annual average Ca^+/Ca column density ratio is 2.4, whereas the limited set of rocket-borne mass spectrometric data indicates that the ratios of Na^+/Na and Fe^+/Fe are only 0.1 and 0.2, respectively (Kopp, 1997; Grebowsky and Aikin, 2002). Thus the ratio of Ca^+/Na^+ is ~0.1, which is reasonably close to the differential ablation ratio of 0.25, indicating that the huge depletion of atomic Ca is due to the metal being more efficiently removed into a permanent sink than Na. The nature of this chemistry has still to be elucidated.

7. Conclusions

The combination of recent satellite observations and ground-based lidar measurements has enabled a near-global climatology of the Na layer to be constructed. The resulting picture illustrates the remarkable way in which the Na layer responds sensitively to many different influences in the upper atmosphere: the flux of interplanetary dust, photochemistry, temperature, the formation of ice clouds, and atmospheric dynamics on a range of scales from gravity waves and tides to inter-hemispheric circulation. Finally, it should be noted that each of the other metals for which there are extensive observations - Fe, K and Ca - behave quite differently from Na (Plane, 2003), providing further tools to probe this fascinating part of the atmosphere.

7. References

Alpers, M., Blix, T., Kirkwood, S., Krankowsky, D., Lübken, F. J., Lutz, S., von Zahn, U. 1st Simultaneous Measurements of Neutral and Ionized Iron Densities in the Upper Mesosphere. J. Geophys. Res. 98, 275-283, 1993.

Bardeen, C. G., Toon, O. B., Jensen, E. J., Marsh, D. R., Harvey, V. L. Numerical simulations of the three-dimensional distribution of meteoric dust in the mesosphere and upper stratosphere. J. Geophys. Res. 113, article no.: D17202, 2008.

Batista, P. P., Clemesha, B. R., Batista, I. S., Simonich, D. M. Characteristics of the Sporadic Sodium Layers Observed at 23^{o}S. J. Geophys. Res. 94, 15349-15358, 1989.

Beatty, T. J., Collins, R. L., Gardner, C. S., Hostetler, C. A., Sechrist, C. F., Tepley, C. A. Simultaneous Radar and Lidar Observations of Sporadic *E* and Na Layers at Arecibo. Geophys. Res. Lett. 16, 1019-1022, 1989.

Bernard, R. Enhancement of the sodium D lines in the twilight sky light. Nature 142, 164-164, 1938.

Bowman, M. R., Gibson, A. J., Sandford, M. C. W. Atmospheric sodium measured by a tuned laser radar. Nature 221, 456-457, 1969.

Ceplecha, Z., Borovicka, J., Elford, W. G., Revelle, D. O., Hawkes, R. L., Porubcan, V., Simek, M. Meteor phenomena and bodies. Space Sci. Rev. 84, 327-471, 1998.

Clemesha, B. R. Sporadic neutral metal layers in the mesosphere and lower thermosphere. J. Atmos. Terr. Phys. 57, 725-736, 1995.

Clemesha, B. R., Kirchhoff, V., Simonich, D. M. Concerning the Seasonal-Variation of the Mesospheric Sodium Layer at Low-Latitudes. Planet Space Sci. 27, 909-910, 1979.

Clemesha, B. R., Kirchhoff, V., Simonich, D. M., Takahashi, H. Evidence of an Extra-Terrestrial Source for Mesospheric Sodium Layer. Geophys. Res. Lett. 5, 873-876, 1978.

Clemesha, B. R., Sahai, Y., Simonich, D. M., Takahashi, H. Nighttime Na-*D* Emission Observed from a Polar-Orbiting DMSP Satellite - Comment. J. Geophys. Res. 95, 6601-6606, 1990.

Clemesha, B. R., Simonich, D. M., Batista, P. P., Batista, I. S. Lidar observations of atmospheric sodium at an equatorial location. J. Atmos. Solar-Terr. Phys. 60, 1773-1778, 1998.

Clemesha, B. R., Simonich, D. M., Batista, P. P., Kirchhoff, V. The Diurnal-Variation of Atmospheric Sodium. J. Geophys. Res. 87, 181-186, 1982.

Clemesha, B. R., Simonich, D. M., Batista, P. P., Vondrak, T., Plane, J. M. C. Negligible long-term temperature trend in the upper atmosphere at 23^{o} S. J. Geophys. Res. 109, article no. D0503, 2004.

Clemesha, B. R., Simonich, D. M., Takahashi, H., Batista, P. P., Sahai, Y. The Annual Variation of the Height of the Atmospheric Sodium Layer at 23^{o} S - Possible Evidence for Convective- Transport. J. Geophys. Res. 97, 5981-5985, 1992a.

Clemesha, B. R., Simonich, D. M., Takahashi, H., Batista, P. P., Sahai, Y. The Annual Variation of the Height of the Atmospheric Sodium Layer at 23^{o}S - Possible Evidence for Convective- Transport. J. Geophys. Res. 97, 5981-5985, 1992b.

Collins, S. C., Plane, J. M. C., Kelley, M. C., Wright, T. G., Soldan, P., Kane, T. J., Gerrard, A. J., Grime, B. W., Rollason, R. J., Friedman, J. S. A study of the role of ion-molecule chemistry in the formation of sporadic sodium layers. J. Atmos. Solar-Terr. Phys. 64, 845-860, 2002.

Cox, R. M., Plane, J. M. C. An experimental and theoretical study of the clustering reactions between Na^+ ions and N_2, O_2 and CO_2. J. Chem. Soc.-Faraday Trans. 93, 2619-2629, 1997.

Cox, R. M., Plane, J. M. C. An ion-molecule mechanism for the formation of neutral sporadic Na layers. J. Geophys. Res. 103, 6349-6359, 1998.

Cox, R. M., Self, D. E., Plane, J. M. C. A study of the reaction between NaHCO3 and H: Apparent closure on the chemistry of mesospheric Na. J. Geophys. Res. 106, 1733-1739, 2001.

Cziczo, D. J., Thomson, D. S., Murphy, D. M. Ablation, flux, and atmospheric implications of meteors inferred from stratospheric aerosol. Science 291, 1772-1775, 2001.

DeLand, M. T., Shettle, E. P., Thomas, G. E., Olivero, J. J. Latitude-dependent long-term variations in polar mesospheric clouds from SBUV version 3 PMC data. J. Geophys. Res. 112, D10315, 2007.

Dyrud, L. P., Denney, K., Urbina, J., Janches, D., Kudeki, E., Franke, S. The meteor flux: It depends how you look. Earth Moon and Planets 95, 89-100, 2005.

Eska, V., Höffner, J., von Zahn, U. Upper atmosphere potassium layer and its seasonal variations at 54^{o} N. J. Geophys. Res. 103, 29207-29214, 1998.

Eska, V., von Zahn, U., Plane, J. M. C. The terrestrial potassium layer (75-110 km) between 71^{o}S and 54^{o}N: Observations and modeling. J. Geophys. Res. 104, 17173-17186, 1999.

Fan, Z. Y., Plane, J. M. C., Gumbel, J. On the global distribution of sporadic sodium layers. Geophys. Res. Lett. 34, article no.: L15808, 2007a.

Fan, Z. Y., Plane, J. M. C., Gumbel, J., Stegman, J., Llewellyn, E. J. Satellite measurements of the global mesospheric sodium layer. Atmos. Chem. Phys. 7, 4107-4115, 2007b.

Fussen, D., Vanhellemont, F., Bingen, C., Kyrola, E., Tamminen, J., Sofieva, V., Hassinen, S., Seppala, A., Verronen, P., Bertaux, J. L., Hauchecorne, A., Dalaudier, F., Renard, J. B., Fraisse, R., d'Andon, O. F., Barrot, G., Mangin, A., Theodore, B., Guirlet, M., Koopman, R., Snoeij, P., Saavedra, L. Global measurement of the mesospheric sodium layer by the star occultation instrument GOMOS. Geophys. Res. Lett. 31, article number: L24110, 2004.

Gabrielli, P., Barbante, C., Plane, J. M. C., Varga, A., Hong, S., Cozzi, G., Gaspari, V., Planchon, F. A. M., Cairns, W., Ferrari, C., Crutzen, P., Cescon, P., Boutron, C. F. Meteoric smoke fallout over the Holocene epoch revealed by iridium and platinum in Greenland ice. Nature 432, 1011-1014, 2004.

Gardner, C. S., Plane, J. M. C., Pan, W. L., Vondrak, T., Murray, B. J., Chu, X. Z. Seasonal variations of the Na and Fe layers at the South Pole and their implications for the chemistry and general circulation of the polar mesosphere. J. Geophys. Res. 110, article no.: D1030210, 2005.

Gardner, C. S., Senft, D. C., Kwon, K. H. Lidar Observations of Substantial Sodium Depletion in the Summertime Arctic Mesosphere. Nature 332, 142-144, 1988.

Gardner, C. S., Voelz, D. G., Sechrist, C. F., Segal, A. C. Lidar Studies of the Nighttime Sodium Layer over Urbana, Illinois .1. Seasonal and Nocturnal Variations. J. Geophys. Res. 91, 3659-3673, 1986.

Gardner, J. A., Broadfoot, A. L., McNeil, W. J., Lai, S. T., Murad, E. Analysis and modeling of the GLO-1 observations of meteoric metals in the thermosphere. J. Atmos. Solar-Terr. Phys. 61, 545-562, 1999.

Gerding, M., Alpers, M., Hoffner, J., von Zahn, U. Sporadic Ca and Ca+ layers at mid-latitudes: Simultaneous observations and implications for their formation. Ann. Geophys. 19, 47-58, 2001.

Gerding, M., Alpers, M., von Zahn, U., Rollason, R. J., Plane, J. M. C. Atmospheric Ca and Ca^+ layers: Midlatitude observations and modeling. J. Geophys. Res. 105, 27131-27146, 2000.

Gibson, A. J., Sandford, M. C. W. The seasonal variation of the night-time sodium layer. J. Atmos. Terr. Phys. 33, 1675-1684, 1971.

Gong, S. S., Yang, G. T., Wang, J. M., Liu, B. M., Cheng, X. W., Xu, J. Y., Wan, W. Occurrence and characteristics of sporadic sodium layer observed by lidar at a mid-latitude location. J. Atmos. Solar-Terr. Phys. 64, 1957-1966, 2002.

Grebowsky, J. M., Aikin, A. C. In situ measurements of meteoric ions, in: Murad, E. ,Williams, I. P. (Eds.), Meteors in the earth's atmosphere. Cambridge University Press, Cambridge, pp. 189-214, 2002.

Grebowsky, J. M., Bilitza, D. Sounding rocket data base of E- and D-region ion composition. Adv. Space Res. 25, 183-192, 1999.

Gumbel, J., Fan, Z. Y., Waldemarsson, T., Stegman, J., Witt, G., Llewellyn, E. J., She, C. Y., Plane, J. M. C. Retrieval of global mesospheric sodium densities from the Odin satellite. Geophys. Res. Lett. 34, article no.: L04813 2007.

Hansen, G., von Zahn, U. Sudden sodium layers in polar latitudes. J. Atmos. Terr. Phys. 52, 585-608, 1990.

Heinselman, C. J. Auroral effects on the gas phase chemistry of meteoric sodium. J. Geophys. Res. 105, 12181-12192, 2000.

Heinselman, C. J., Thayer, J. P., Watkins, B. J. A high-latitude observation of sporadic sodium and sporadic *E* layer formation. Geophys. Res. Lett. 25, 3059-3062, 1998.

Helmer, M., Plane, J. M. C., Qian, J., Gardner, C. S. A model of meteoric iron in the upper atmosphere. J. Geophys. Res. 103, 10913-10925, 1998.

Höffner, J., Lübken, F. J. Potassium lidar temperatures and densities in the mesopause region at Spitsbergen (78^{o} N). J. Geophys. Res. 112, article no.: D20114, 2007.

Hughes, D. W. Meteors and cosmic dust. Endeavour 21, 31-35, 1997.

Hunten, D. M. Spectroscopic studies of the twilight airglow. Space Sci. Rev. 6, 493-573, 1967.

Hunten, D. M., Turco, R. P., Toon, O. B. Smoke and dust particles of meteoric origin in the mesosphere and stratosphere. J. Atmos. Sci. 37, 1342-1357, 1980.

Janches, D., Heinselman, C. J., Chau, J. L., Chandran, A., Woodman, R. Modeling the global micrometeor input function in the upper atmosphere observed by high power and large aperture radars. J. Geophys. Res. 111, article no.: A07317, 2006.

Janches, D., Mathews, J. D., Meisel, D. D., Zhou, Q. H. Micrometeor observations using the Arecibo 430 MHz radar I. Determination of the ballistic parameter from measured Doppler velocity and deceleration results. Icarus 145, 53-63, 2000.

Kalashnikova, O., Horanyi, M., Thomas, G. E., Toon, O. B. Meteoric Smoke production in the atmosphere. Geophys. Res. Lett. 27, 3293-3296, 2000.

Kane, T. J., Gardner, C. S. Structure and Seasonal Variability of the Nighttime Mesospheric Fe Layer at Midlatitudes. J. Geophys. Res. 98, 16875-16886, 1993.

Kane, T. J., Gardner, C. S., Zhou, Q., Mathews, J. D., Tepley, C. A. Lidar, Radar and Airglow Observations of a Prominent Sporadic Na Sporadic-E Layer Event at Arecibo During Aida-89. J. Atmos. Terr. Phys. 55, 499-511, 1993.

Kane, T. J., Hostetler, C. A., Gardner, C. S. Horizontal and Vertical Structure of the Major Sporadic Sodium Layer Events Observed During Aloha-90. Geophys. Res. Lett. 18, 1365-1368, 1991.

Kopp, E. On the abundance of metal ions in the lower ionosphere. J. Geophys. Res. 102, 9667-9674, 1997.

Kurzawa, H., von Zahn, U. Sodium Density and Atmospheric-Temperature in the Mesopause Region in Polar Summer. J. Atmos. Terr. Phys. 52, 981-993, 1990.

Kwon, K. H., Senft, D. C., Gardner, C. S. Lidar Observations of Sporadic Sodium Layers at Mauna-Kea-Observatory, Hawaii. J. Geophys. Res. 93, 14199-14208, 1988.

Lanci, L., Kent, D. V., Biscaye, P. E. Meteoric smoke concentration in the Vostok ice core estimated from superparamagnetic relaxation and some consequences for estimates of Earth accretion rate. Geophys. Res. Lett. 34, article no.: L10803, 2007.

Love, S. G., Brownlee, D. E. A direct measurement of the terrestrial mass accretion rate of cosmic dust. Science 262, 550-553, 1993.

Mason, J. Handbook of Elemental Abundances of the Elements in Meteorites, Gordon and Breach, Newark, NJ, 1971.

Mathews, J. D., Zhou, Q., Philbrick, C. R., Morton, Y. T., Gardner, C. S. Observations of ion and sodium layer coupled processes during AIDA. J. Atmos. Terr. Phys. 55, 487-498, 1993.

McNeil, W. J., Lai, S. T., Murad, E. Differential ablation of cosmic dust and implications for the relative abundances of atmospheric metals. J. Geophys. Res. 103, 10899-10911, 1998.

McNeil, W. J., Murad, E., Plane, J. M. C. Models of meteoric metals in the atmosphere, in: Murad, E. ,Williams, I. P. (Eds.), Meteors in the Earth's Atmosphere. Cambridge University Press, Cambridge, pp. 265-287, 2002.

Megie, G., Blamont, J. E. Laser Sounding of Atmospheric Sodium Interpretation in Terms of Global Atmospheric Parameters. Planet. Space Sci. 25, 1093-1109, 1977.

Megner, L., Rapp, M., Gumbel, J. Distribution of meteoric smoke - sensitivity to microphysical properties and atmospheric conditions. Atmos. Chem. Phys. 6, 4415-4426, 2006.

Murray, B. J., Plane, J. M. C. Uptake of Fe, Na and K atoms on low-temperature ice: implications for metal atom scavenging in the vicinity of polar mesospheric clouds. Phys. Chem. Chem. Phys. 7, 3970-3979, 2005.

Nagasawa, C., Abo, M. Lidar Observations of a Lot of Sporadic Sodium Layers in Midlatitude. Geophys. Res. Lett. 22, 263-266, 1995.

Newman, A. L. Nighttime Na *D* emission observed from a polar-orbiting DMSP satellite. J. Geophys. Res. 93, 4067-4075, 1988.

Plane, J. M. C. The Chemistry of Meteoric Metals in the Earths Upper Atmosphere. Int. Rev. Phys. Chem. 10, 55-106, 1991.

Plane, J. M. C. Laboratory studies of meteoric metal chemistry, in: Murad, E. ,Williams, I. P. (Eds.), Meteors in the Earth's Atmosphere. Cambridge University Press, Cambridge, pp. 289-309, 2002.

Plane, J. M. C. Atmospheric chemistry of meteoric metals. Chem. Rev. 103, 4963-4984, 2003.

Plane, J. M. C. A time-resolved model of the mesospheric Na layer: constraints on the meteor input function. Atmos. Chem. Phys. 4, 627-638, 2004.

Plane, J. M. C., Cox, R. M., Qian, J., Pfenninger, W. M., Papen, G. C., Gardner, C. S., Espy, P. J. Mesospheric Na layer at extreme high latitudes in summer. J. Geophys. Res. 103, 6381-6389, 1998a.

Plane, J. M. C., Cox, R. M., Qian, J., Pfenninger, W. M., Papen, G. C., Gardner, C. S., Espy, P. J. Mesospheric Na layer at extreme high latitudes in summer. J. Geophys. Res. 103, 6381-6389, 1998b.

Plane, J. M. C., Gardner, C. S., Yu, J. R., She, C. Y., Garcia, R. R., Pumphrey, H. C. Mesospheric Na layer at 40 degrees N: Modeling and observations. J. Geophys. Res. 104, 3773-3788, 1999.

Plane, J. M. C., Plowright, R. J., Wright, T. G. A theoretical study of the ion-molecule chemistry of $K^+.X$ complexes (X = O, O_2, N_2, CO_2, H_2O): Implications for the upper atmosphere. J. Phys. Chem. A 110, 3093-3100, 2006.

Raizada, S., Tepley , C. A. Seasonal variation of mesospheric iron layers at Arecibo: First results from low-latitudes. Geophys. Res. Lett. 30, 1082-1085, 2003.

Saunders, R. W., Plane, J. M. C. A laboratory study of meteor smoke analogues: Composition, optical properties and growth kinetics. J. Atmos. Solar-Terr. Phys. 68, 2182-2202, 2006.

Scharringhausen, M., Aikin, A. C., Burrows, J. P., Sinnhuber, M. Global column density retrievals of mesospheric and thermospheric MgI and MgII from SCIAMACHY limb and nadir radiance data. J. Geophys. Res. 113, article no.: D13303, 2008.

Sears, D. W., Dodd, R. T. Overview and Classification of Meteorites, in: Kerridge, J. F. ,Matthews, M. S. (Eds.), Meteorites and the Early Solar System. University of Arizona Press, Tucson, 1988.

She, C. Y., S.S. Chen, Z.L. Hu, J. Sherman, J.D. Vance, V. Vasoli, M.A. White, J.R. Yu, and D.A. Krueger. Eight-year climatology of nocturnal temperature and sodium density in the mesopause region (80 to 105 km) over Fort Collins, CO (41^{o} N, 105^{o} W). Geophys. Res. Lett. 27 3289-3292, 2000.

Simonich, D. M., Clemesha, B. R., Kirchhoff, V. W. J. H. Mesospheric sodium layer at 23^{o} S - nocturnal and seasonal variations. J. Geophys. Res. 84, 1543-1550, 1979.

Slipher, V. M. Emissions in the spectrum of the light of the night sky. Publ. Astron. Soc. Pacific 41, 262-263, 1929.

States, R. J., Gardner, C. S. Structure of the mesospheric Na layer at 40 degrees N latitude: Seasonal and diurnal variations. J. Geophys. Res. 104, 11783-11798, 1999.

States, R. J., Gardner, C. S. Thermal structure of the mesopause region (80-105 km) at 40 degrees N latitude. Part I: Seasonal variations. J. Atmos. Sci. 57, 66-77, 2000.

Vondrak, T., Plane, J. M. C., Broadley, S. L., Janches, D. A chemical model of meteoric ablation. Atmos. Chem. Phys. 8, 1-17, 2008.

Williams, B. P., Berkey, F. T., Sherman, J., She, C. Y. Coincident extremely large sporadic sodium and sporadic E layers observed in the lower thermosphere over Colorado and Utah. Annal. Geophys. 25, 3-8, 2007.

Williams, I. P. The evolution of meteoroid streams, in: Murad, E. ,WIlliams, I. P. (Eds.), Meteors in the earth's atmosphere. Cambridge University Press, Cambridge, pp. 2-32, 2002.

Yi, F., Yu., C., Zhang, S., Yue, X., He, Y., Huang, C., Zhang, Y., Huang, K. Seasonal variations of the nocturnal mesospheric Na and Fe layers at 30^{o}N. J. Geophys. Res. 114, article no.: D010344, 2009.

Yuan, T., She, C. Y., Hagan, M. E., Williams, B. P., Li, T., Arnold, K., Kawahara, T. D., Acott, P. E., Vance, J. D., Krueger, D., Roble, R. G. Seasonal variation of diurnal perturbations in mesopause region temperature, zonal, and meridional winds above Fort Collins, Colorado (40.6^{o}N, 105^{o}W). J. Geophys. Res. 111, article no.: D06103, 2006.

Table 1. Monthly column density of the atomic Na layer as a function of latitude (units: 10^9 atom cm^{-2}). Italicised entries are extrapolated values used for the contour plot in Figure 5.

Lat.	Jan	Feb	Mar	Apr	May	Jun	Jul	Aug	Sep	Oct	Nov	Dec
90	*6.00*	*5.00*	*4.00*	*2.00*	*1.30*	*0.60*	*0.40*	*1.20*	*4.20*	*6.00*	*6.00*	*5.90*
80	*5.40*	*5.00*	4.63	2.35	1.72	0.64	0.33	1.59	4.24	*6.00*	*5.90*	*5.80*
70	*5.00*	5.05	4.99	2.56	2.08	1.10	0.92	2.12	4.61	5.76	5.80	*5.70*
60	*5.90*	5.86	5.06	2.83	2.21	1.45	1.58	2.59	4.29	5.82	5.80	*5.70*
50	*5.60*	5.70	4.72	2.71	2.15	1.97	2.13	3.00	4.07	5.69	6.19	*5.90*
40	5.12	4.78	3.94	3.20	2.66	2.86	2.94	3.25	3.44	5.80	5.80	5.04
30	*4.70*	4.36	3.62	3.66	3.36	3.41	3.37	3.39	3.63	5.65	5.43	3.58
20	*4.50*	4.09	2.90	3.87	3.75	3.45	3.43	3.14	3.55	4.90	4.59	3.66
10	3.57	3.88	2.46	3.43	3.44	3.09	3.21	2.96	3.47	3.95	3.69	3.44
0	3.58	3.70	1.89	2.33	2.94	2.87	3.02	2.84	3.03	3.50	3.71	3.48
-10	3.36	3.67	2.30	2.13	2.49	2.65	2.69	2.79	2.95	3.60	3.68	3.45
-20	3.26	3.74	2.48	2.19	5.80	5.75	5.85	5.40	5.00	4.85	3.70	3.45
-30	3.11	3.28	2.97	*4.70*	*5.90*	*5.90*	*5.90*	*5.40*	4.37	4.58	3.72	3.14
-40	2.82	3.52	3.09	*5.00*	*6.00*	*6.00*	*6.00*	*5.50*	4.64	4.02	3.45	2.61
-50	2.60	3.47	4.26	*5.50*	*6.20*	*6.20*	*6.20*	*5.70*	4.91	3.51	3.05	2.04
-60	1.93	2.46	4.66	*5.70*	*6.40*	*6.50*	*6.40*	*5.80*	4.80	3.38	2.52	1.50
-70	1.32	1.96	5.66	*6.00*	*6.50*	*7.00*	*6.50*	*6.00*	4.39	3.21	1.90	1.08
-80	0.93	1.35	*3.00*	*6.00*	*6.50*	*7.30*	*6.50*	*6.20*	*4.50*	3.18	1.70	0.80
-90	0.70	1.27	2.96	5.25	6.72	7.42	7.17	6.57	6.16	4.66	2.34	0.90

Table 2. Monthly peak density of the atomic Na layer (units: 10^3 atom cm^{-3})

Lat.	Jan	Feb	Mar	Apr	May	Jun	Jul	Aug	Sep	Oct	Nov	Dec
90												
80			3.99	2.01	1.88	1.16	0.77	2.14	4.14	6.83		
70		3.84	4.06	2.41	2.47	1.52	1.31	2.54	4.49	4.89		
60		4.61	4.16	2.53	2.27	1.59	1.66	2.40	3.95	5.25		
50		4.26	3.67	2.30	1.85	1.75	1.84	2.41	3.56	5.17	4.53	
40		3.51	3.03	2.59	2.14	2.28	2.30	2.48	3.06	4.78	4.25	
30		3.11	2.68	2.82	2.54	2.61	2.58	2.61	3.09	4.68	3.91	2.77
20		3.09	2.28	2.91	2.90	2.52	2.56	2.33	2.79	4.18	3.64	2.66
10	3.10	3.07	2.10	2.74	2.45	2.41	2.37	2.24	2.75	3.68	3.20	2.46
0	2.86	3.86	1.56	2.12	2.29	2.01	2.14	2.27	2.46	3.10	2.96	2.18
-10	2.38	2.41	1.79	2.02	1.97	2.16	1.73	2.41	2.61	3.19	2.61	2.08
-20	2.32	2.58	1.96	1.75				2.41	2.84	3.92	2.97	2.38
-30	2.18	2.18	2.25						3.30	3.68	2.71	2.19
-40	2.03	2.68	2.21						3.54	3.43	2.73	1.94
-50	1.97	2.82	4.61						3.47	3.16	2.69	1.71
-60	2.01	2.55	6.26						3.67	3.06	2.42	1.60
-70	1.61	2.18	5.76						3.64	2.83	2.03	1.34
-80	1.43	1.79							3.49	3.15	1.88	1.20
-90	1.54	1.99	3.51	5.14	5.74	5.51	5.22	5.20	5.27	4.03	2.20	1.62

Table 3. Monthly peak height of the atomic Na layer (units: km)

Lat.	Jan	Feb	Mar	Apr	May	Jun	Jul	Aug	Sep	Oct	Nov	Dec
90												
80			90.3	92.3	91.6	91.5	92.0	92.8	91.4	88.4		
70		90.2	89.9	92.4	91.7	91.0	91.2	91.9	90.8	91.0		
60		89.2	90.4	92.1	90.9	90.1	90.6	91.1	90.9	90.0		
50		90.7	90.9	91.0	89.7	90.0	90.1	91.1	91.1	90.2	90.0	
40		91.6	91.3	91.0	89.2	90.2	90.3	91.3	91.7	91.0	90.8	
30		92.4	91.1	91.0	90.2	90.4	90.7	91.6	91.3	89.9	90.9	
20		92.1	92.1	90.8	91.4	91.0	91.3	92.2	91.9	91.2	92.0	91.1
10	90.0	91.4	92.2	91.7	92.6	91.3	91.4	92.7	92.0	92.8	92.2	92.3
0	92.1	90.7	92.9	92.4	92.8	92.4	92.1	93.2	92.3	92.5	92.1	93.0
-10	92.2	92.8	93.5	92.2	92.8	92.6	91.9	92.9	92.2	92.8	92.6	92.8
-20	91.5	92.2	93.1	92.6	91.8	91.6	91.6	91.6	92.0	91.9	90.5	91.4
-30	90.9	92.0	92.0						91.4	90.2	90.3	91.3
-40	90.4	90.8	91.8						91.9	91.7	90.7	91.0
-50	90.8	90.7	90.5						90.9	92.6	91.5	90.8
-60	91.5	90.6	91.0						90.0	92.4	91.8	91.8
-70	91.8	91.1	93.0						90.0	92.5	92.5	92.4
-80	92.1	91.3							90.4	92.0	92.9	93.1
-90	93.6	93.0	91.1	90.1	88.7	89.2	89.4	89.8	88.5	88.0	93.6	93.7

Table 4. Full-width at half maximum of the atomic Na layer between 80 and 110 km (units: km)

Lat.	Jan	Feb	Mar	Apr	May	Jun	Jul	Aug	Sep	Oct	Nov	Dec
90												
80			8.85	8.19	7.49	5.55	4.83	5.88	6.56	6.87		
70		9.10	8.85	8.16	7.63	6.48	5.62	6.70	6.55	6.87		
60		9.09	8.95	8.38	8.01	7.51	7.18	8.33	6.60	6.87		
50		9.06	8.95	8.68	8.32	7.95	8.60	8.97	6.72	6.86	7.25	
40		8.96	8.79	8.66	8.49	8.46	9.50	8.92	6.38	6.88	7.21	
30		8.90	9.07	8.94	8.68	8.30	9.16	8.23	6.46	6.89	7.20	
20		8.84	8.80	8.97	8.57	8.30	9.25	7.12	6.46	6.80	7.03	7.79
10	9.60	8.78	8.58	8.73	8.34	8.02	8.79	6.70	6.35	6.75	7.09	7.76
0	9.57	8.82	8.31	8.17	8.17	8.01	7.64	6.01	6.17	6.74	7.07	7.76
-10	9.42	8.67	8.85	8.56	8.20	7.61	5.75	5.66	6.14	6.87	7.05	7.67
-20	9.92	8.95	8.96	8.94				5.12	6.35	6.86	7.27	7.87
-30	9.94	8.80	8.98						6.59	6.93	7.10	7.59
-40	8.78	8.48	9.05						6.59	6.88	6.96	7.31
-50	8.32	8.20	9.04						6.56	6.80	6.77	7.00
-60	6.94	7.20	9.06						6.55	6.80	6.61	6.35
-70	6.43	6.81	9.08						6.41	6.80	6.34	5.98
-80	5.14	5.95							6.22	6.67	6.13	5.54
-90	4.31	6.14	7.9	8.9	10.2	12.9	13.1	12.0	11.0	11.3	10.8	3.91

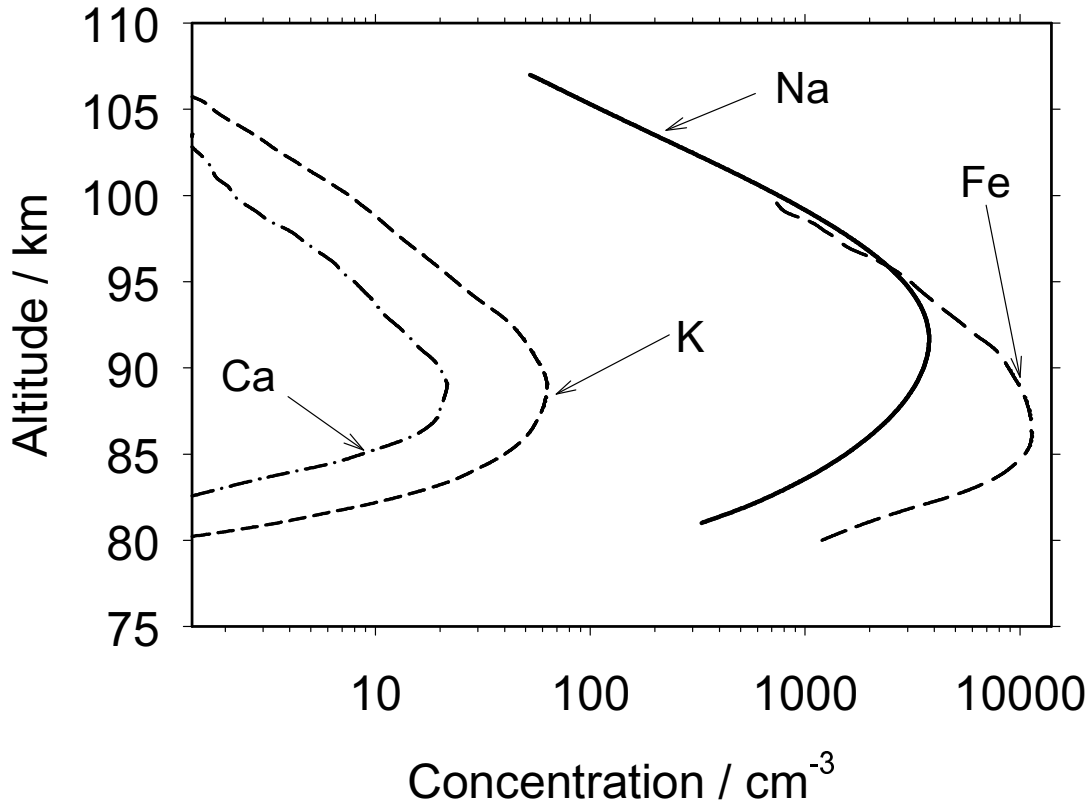

Figure 1. Vertical profiles of the annual mean concentrations at northern hemisphere mid-latitudes of: Na (Plane, J. M. C. et al. J. Geophys. Res. 104, 3773-3788, 1999); Fe (Helmer, M. et al. J. Geophys. Res. 103, 10913-10925, 1998.); K (Eska, V. et al. J. Geophys. Res. 104, 17173-17186, 1999); and Ca (Gerding, M. et al. J. Geophys. Res. 105, 27131-27146, 2000).

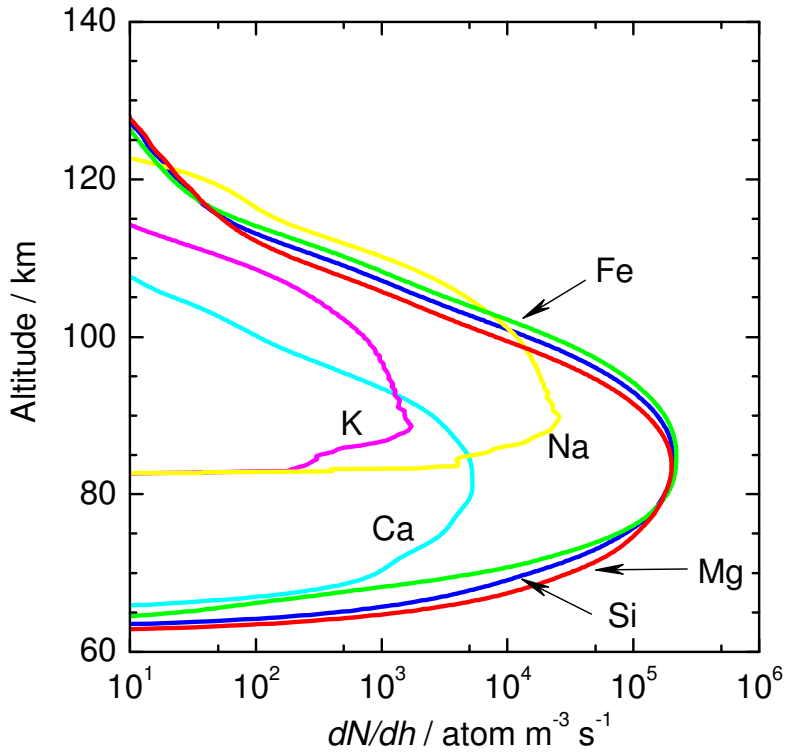

Figure 2. Injection rates of individual elements, integrated over the distributions of meteoroid mass (5 x 10^{-18} – 5 x 10^{-3} g) and velocity (11.5 – 72.5 km s^{-1}) from the *Long Duration Exposure Facility* experiment. These injection rates correspond to a total meteoroid input of ~90 t d^{-1} into the atmosphere.

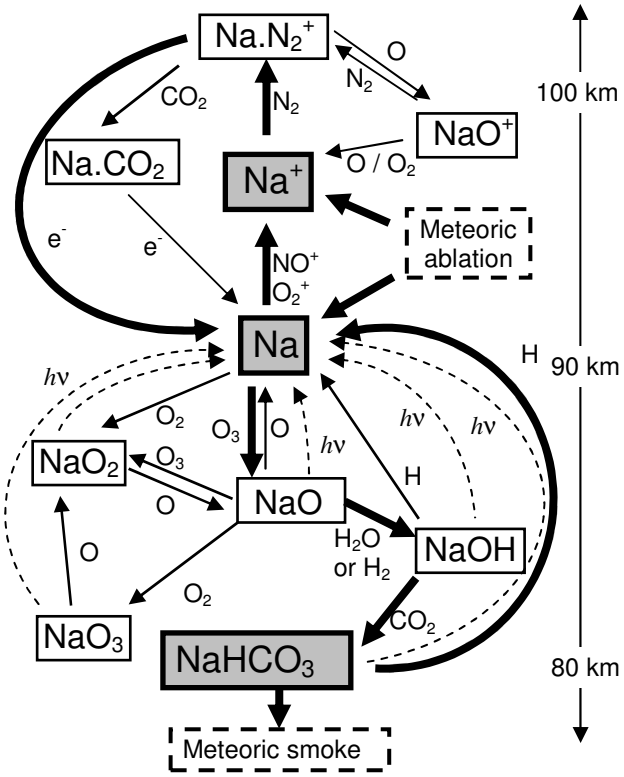

Figure 3. Sodium chemistry in the mesosphere and lower thermosphere. The major sodium species are in grey-filled boxes, and the dominant chemical pathways are shown with thick solid arrows.

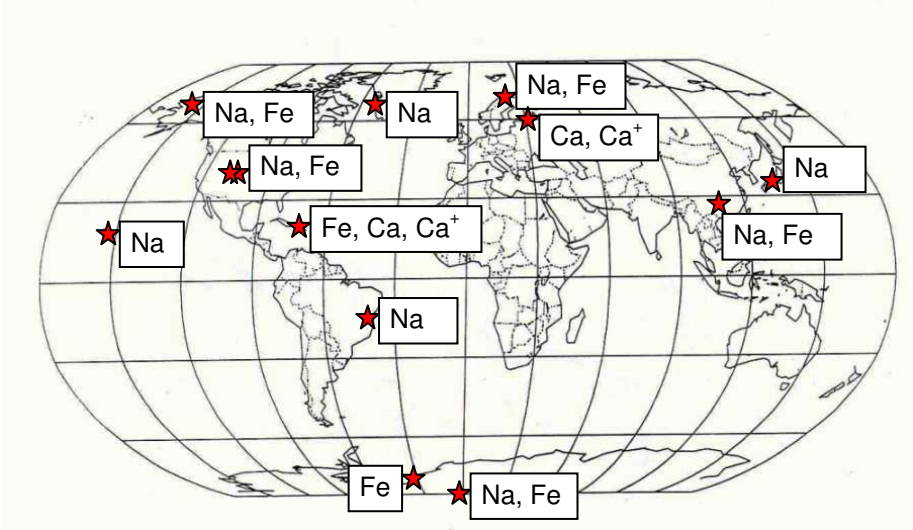

Figure 4. Locations of ground-based metal resonance lidar observatories with significant records on Na, Fe, Ca and Ca^+. FtC = Fort Collins; Kb=Kühlungsborn

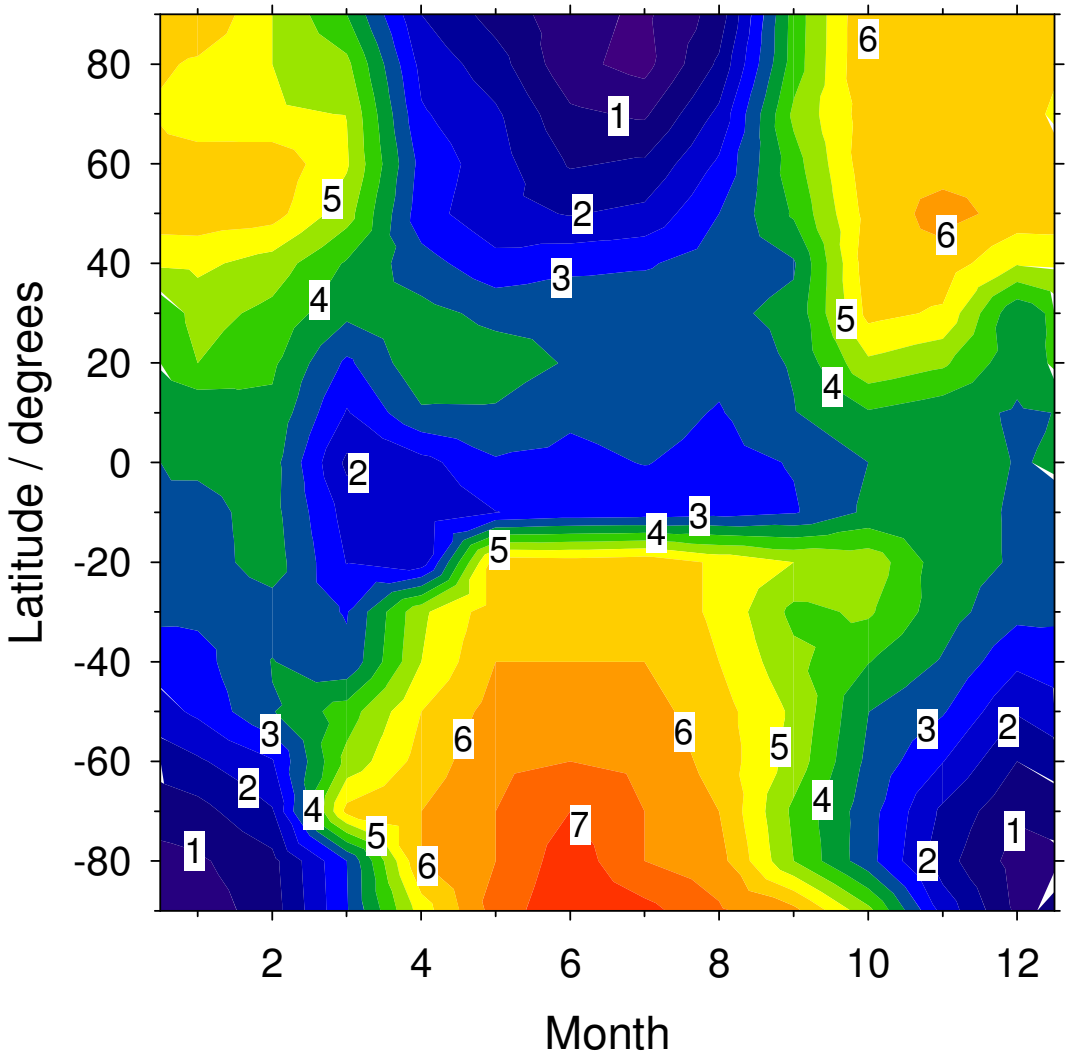

Figure 5. Column abundance of the Na layer (units: 10^9 atom cm^{-2}) as a function of latitude and month.

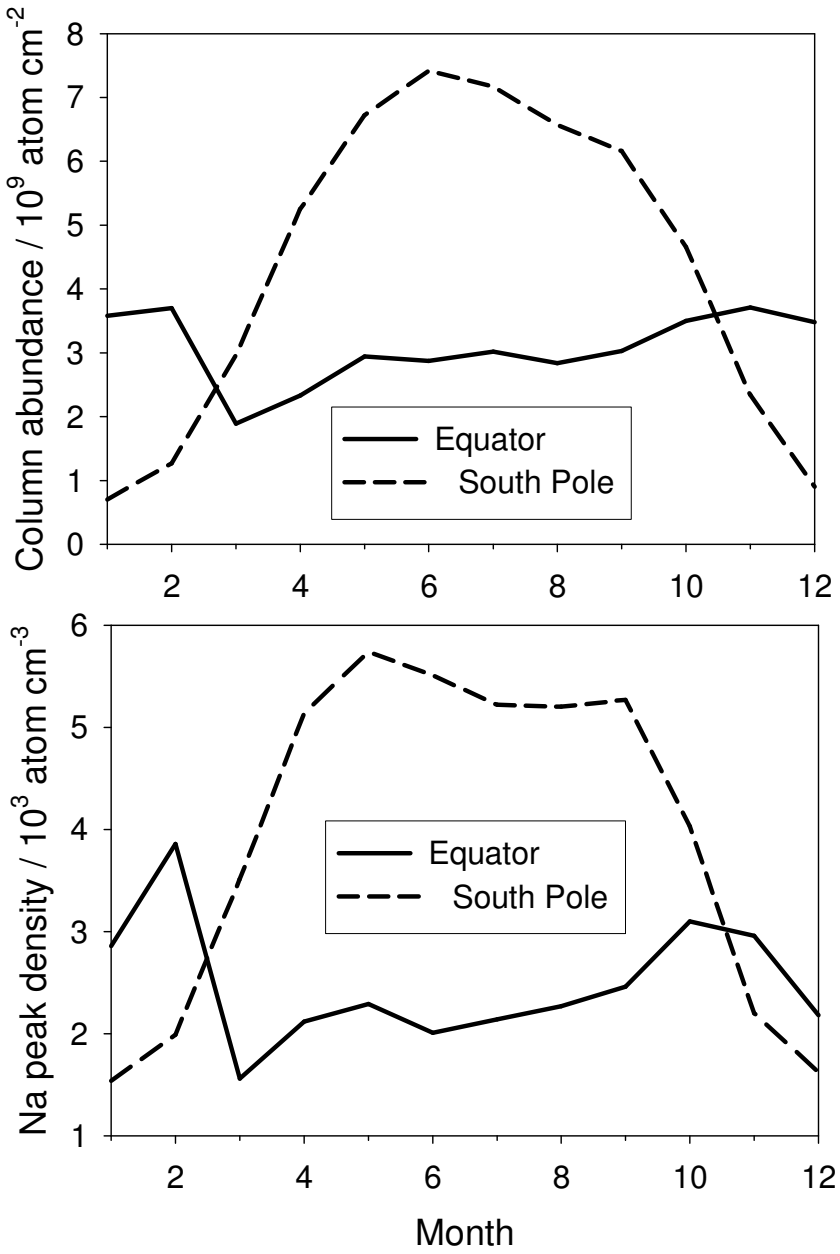

Figure 6. Column abundance (top panel) and peak density (bottom panel) of the Na layer as a function of month at the equator and South Pole.

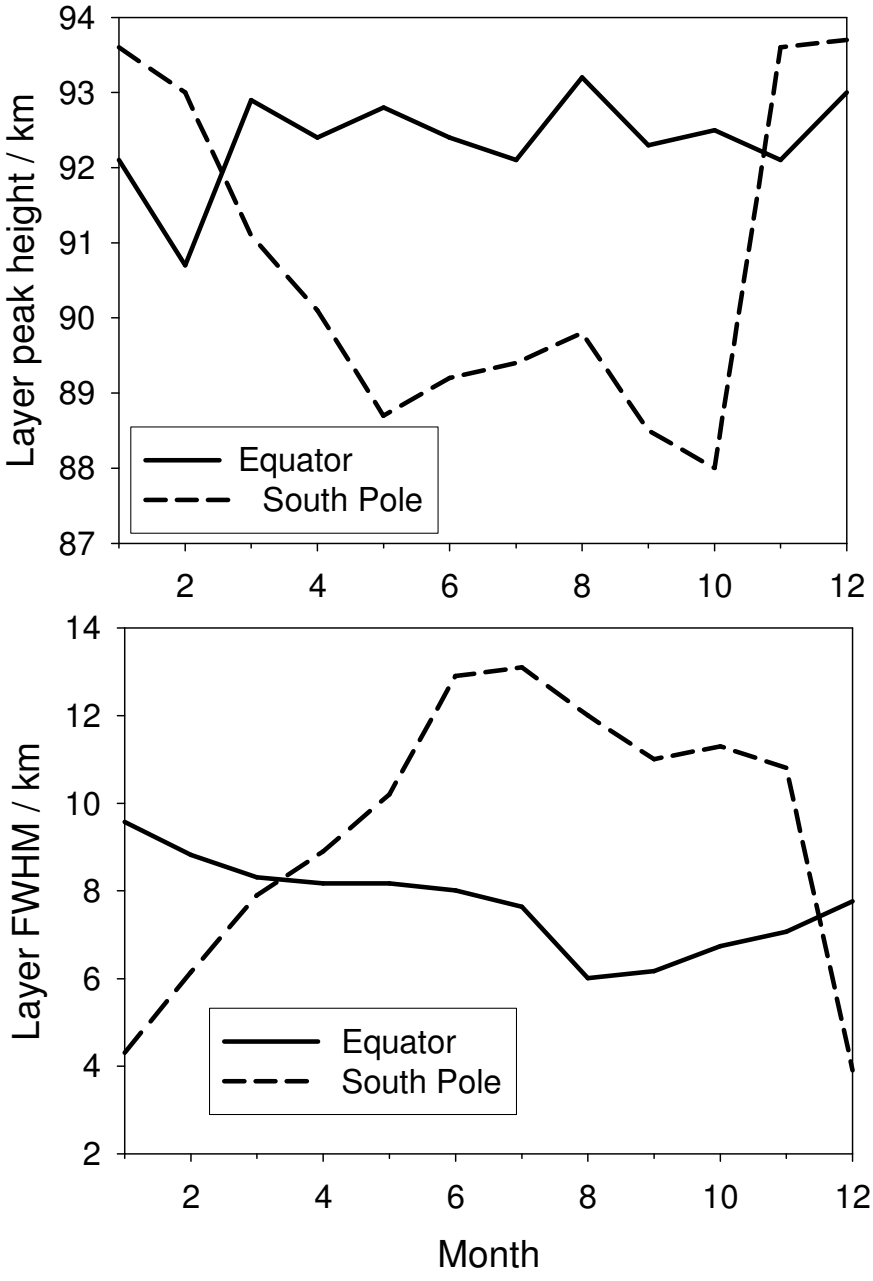

Figure 7. Peak height (top panel) and FWHM (bottom panel) of the Na layer as a function of month at the equator and South Pole.

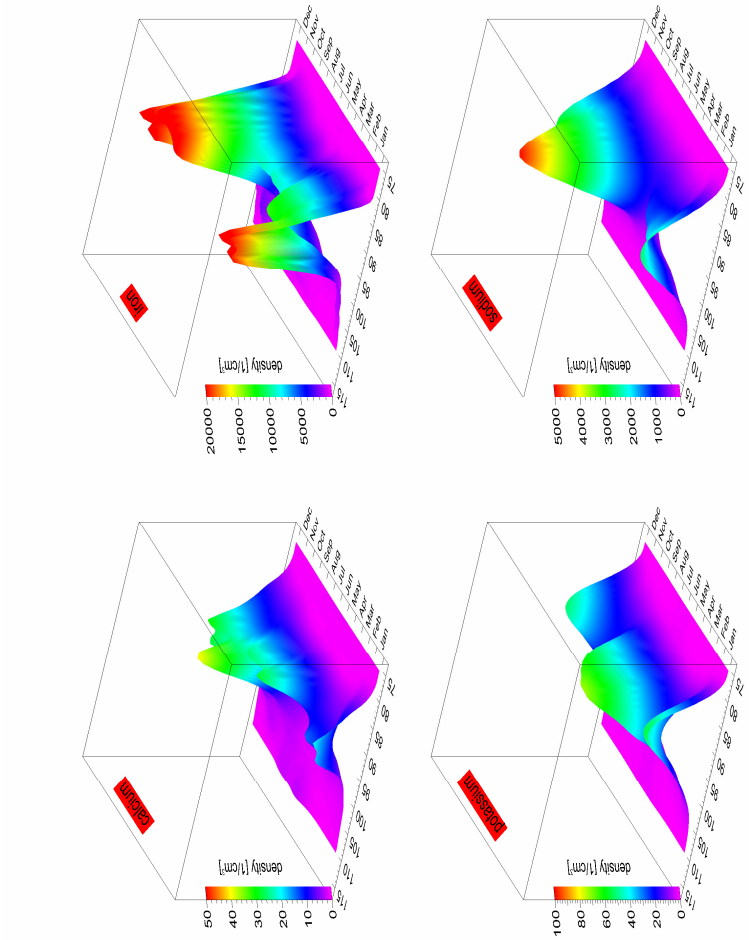

Figure 8. Three-dimensional mesh plots of the annual variations of the Ca, Fe , K and Na layers, measured by lidar at mid-latitude sites in the U.S. and Europe (see the caption to Figure 1 for details). Reproduced with permission from Gerding, M. et al. *J. Geophys. Res.* **2000**, *105*, 27131.